When the dust has settled: Calculation of binding affinities from first principles for SARS-CoV-2 variants with quantitative accuracy

Emma Goulard Coderc de Lacam,^{†,‡} Marharyta Blazhynska,^{†,¶} Haochuan Chen,[†] James C. Gumbart,*,§ and Christophe Chipot*,^{†,||,⊥}

†Laboratoire International Associé Centre National de la Recherche Scientifique et University of Illinois at Urbana-Champaign, Unité Mixte de Recherche n°7019, Université de Lorraine, B.P. 70239, 54506 Vandœuvre-lès-Nancy cedex, France

‡Contributed equally to this study

¶*Contributed equally to this study*

§School of Physics, Georgia Institute of Technology, Atlanta, Georgia 30332, USA

||Theoretical and Computational Biophysics Group, Beckman Institute, and Department of
Physics, University of Illinois at Urbana-Champaign, Urbana, USA

\(\triangle Department of Biochemistry and Molecular Biology, The University of Chicago, 929 E. 57th

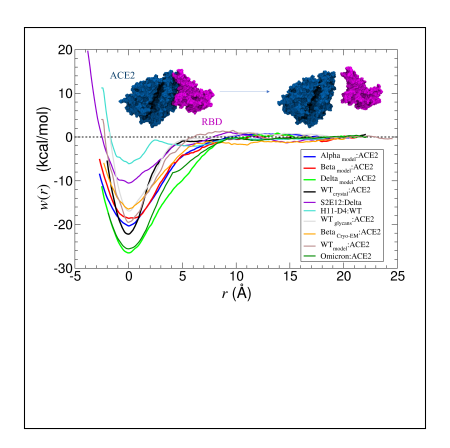
Street W225, Chicago, Illinois 60637, USA

E-mail: gumbart@physics.gatech.edu; chipot@illinois.edu

Abstract

Accurate determination of binding free energy is pivotal for the study of many biological processes and has been applied in a number of theoretical investigations to compare the affinity of SARS-CoV-2 variants towards the host cell. Diversity of these variants challenges the development of effective general therapies, their transmissibility relying either on an increased affinity towards their dedicated human receptor, the angiotensin-converting enzyme 2 (ACE2), or on escaping the immune response. Now that robust structural data are available, we have determined with utmost accuracy the standard binding free energy of the receptor-binding domain (RBD) to the most widespread variants, namely Alpha, Beta, Delta, Omicron BA.2 as well as the wild type (WT) in complex either with ACE2 or with antibodies, viz, S2E12 and H11-D4, using a rigorous theoretical framework that combines molecular dynamics and potential-of-mean-force calculations. Our results show that an appropriate starting structure is crucial to ensure appropriate reproduction of the binding affinity, allowing the variants to be compared. They also emphasize the necessity to apply the relevant methodology, bereft of any shortcut, to account for all the contributions to the standard binding free energy. Our estimates of the binding affinities support the view that whereas the Alpha and Beta variants lean on an increased affinity towards the host cell, the Delta and Omicron BA.2 variants choose immune escape. Moreover, the S2E12 antibody, already known to be active against the WT (Starr et al., 2021; Mlcochova et al., 2021) proved to be equally effective against the Delta variant. In stark contrast, H11-D4 retains a low affinity towards the WT, compared to that of ACE2 for the latter. Assuming robust structural information, the methodology employed herein successfully addresses the challenging protein-protein binding problem in the context of coronavirus disease 2019, while offering promising perspectives for predictive studies of ever-emerging variants.

TOC Graphic



Introduction

Severe acute respiratory syndrome coronavirus 2 (SARS-CoV-2), originated from Wuhan, China, in late December 2019, ³ is the virus that causes coronavirus disease 2019, or COVID-19, which has quickly escalated into a worldwide syndemic ⁴ and resulted in more than six million casualties. ⁵ This virion particle is composed of a nucleocapsid, membrane, spike (S), and envelope structural proteins. The cell entry is mediated through the S protein, which can be decomposed into two subunits, S1 and S2. ^{6–8} The first subunit contains the receptor-binding domain (RBD) responsible for the binding to the human receptor, the angiotensin convertor enzyme 2 (ACE2), ^{9,10} whereas the second subunit contains the cell fusion machinery and serves as an anchor to the membrane. A cleavage between the two subunits is necessary for infection, and is performed in host cells by enzymes, e.g., furin, prior to release. ^{11,12}

The virus keeps on mutating with new variants appearing on the World Health Organization (WHO) watch list, referred to as variants of concern (VOCs), thereby hampering the discovery of efficient therapies. ^{13–15} According to the Centers for Disease Control and Prevention (CDC), VOCs are characterized by either an increase in transmissibility, a more severe disease (i.e., more casualties, higher hospitalization rates), a reduced neutralization by antibodies, and reduced effectiveness of treatments, vaccines, or detection failures. ¹⁶

Several mutations that confer a higher reproduction rate have been reported for the different variants. D614G, in particular, is known to promote S1/S2 cleavage, allowing a more exposed RBD, which favors binding to ACE2. ^{17,18} However, this mutation has been found in many variants, including all the VOCs, and cannot be the sole cause of the fitness difference between them. In general, mutations in the virus can improve two properties, pivotal for higher infectivity, namely binding to ACE2 via its RBD, ^{6,9,10,19} or escaping the immune response. ^{20,21}

State-of-the-art free-energy calculations could play a crucial role in the quantitative prediction of binding affinities, and, thereupon, their comparison for the different VOCs binding through their

RBDs to either ACE2, or a series of antibodies. One possible route to investigate how structural differences between VOCs affect recognition and association to the host cell consists in assessing relative binding affinities to ACE2 through in-silico point mutations^{22–24} by means of alchemical transformations. ^{25,26} For instance, one of the rigorous studies of the mutation of N501 was performed by Fratev²³ using free-energy perturbation (FEP) calculations. ^{27–29} In this computational investigation, the N501Y substitution, observed in the Alpha variant, led to an enhanced affinity by 1.8 kcal/mol, compared to the wild-type (WT), a finding in line with that of Pavlova et al. using a similar strategy. ³⁰ Additional predictive in-silico point mutations were carried out in VOCs, although they have yet to be documented thoroughly at the experimental level. ^{6,31,32}

The limitation of relative binding free-energy calculations lies in their provision of a binding-affinity difference based on a reference state. In other words, for a relative binding free-energy calculation, the reference state must be known beforehand. To circumvent this limitation, resorting to absolute binding free-energy calculations might be desirable. For instance, as a first step towards the quantitative assessment of the thermodynamics that underlies molecular association, Kim et al. turned to steered molecular dynamics (SMD)³³ to estimate the difference in binding strength for all the VOCs available at the time of their study. They showed that the force needed to separate the Alpha variant RBD from ACE2 is the strongest amongst all investigated VOCs. In contrast, the difference in the force profiles between the WT and the Beta or Delta variant is marginal. These observations were experimentally validated by Koehler et al. 55 employing atomic force microscopy, 6 barring the Delta variant, which was not considered in their study. It is worth noting that SMD can, in principle, offer access to the binding free energy at the price of multiple realizations in a near-equilibrium regime, and application of the Jarzynski identity, 37,38 which was not performed by Kim et al. 34

Conversely, potential-of-mean-force (PMF) calculations represent another option relying on first principles to obtain accurate binding affinities. García-Iriepa et al.³⁹ used a $1-\mu s$ simulation with the metadynamics-extended adaptive biasing force (meta-eABF) algorithm⁴⁰ to determine

a binding free-energy of about -2.6 kcal/mol between the WT RBD and ACE2, suggestive of a rather innocuous viral load. Ngo et al.⁴¹ estimated the energetic cost to fully dissociate the RBD from ACE2 to be 15 kcal/mol, while Chakraborty obtained a binding free-energy estimate of -34 kcal/mol,⁴² turning to umbrella sampling⁴³ combined with the weighted histogram analysis method.^{44,45} These discrepant results, at variance with the experimental findings, ¹⁰ may be ascribed to insufficient sampling, most notably to account for the slow reorientation of the binding partners, as well as premature and possibly incomplete structural data.

Another popular approach for the determination of absolute binding free energies is provided by molecular mechanics/Poisson-Boltzmann surface area (MM/PBSA), or molecular mechanics/ generalized Born surface area (MM/GBSA)^{46–50} because of its inexpensive appealing nature. However, this methodology has proven at times to grossly overestimate standard binding affinities. ^{51–53} For instance, in the case of the WT:ACE2 complex examined by Khan et al., the binding affinity amounted to –64.0 kcal/mol, ⁵⁴ at variance with the experimental data obtained by Lan et al. of –11.4 kcal/mol. ¹⁰ In all likelihood, both MM/PBSA and MM/GBSA are also vulnerable to the sampling issues and limitations of the structural data mentioned previously.

The present contribution aims to predict from first principles, with accurate structural data, the absolute binding free energies between the RBD of a number of SARS-CoV-2 VOCs and (i) the ACE2 protein and (ii) neutralizing antibodies, following the rigorous theoretical framework of the geometrical route, ^{55,56} to elucidate the role of point mutations in viral contagiousness. The RBDs investigated here are those of the WT, the Alpha variant (December 2020), the Beta variant (December 2020), the Delta variant (May 2021), and Omicron BA.2 (November 2021). ¹³ The latter is known to spread faster than Delta and was categorized as a VOC within only a few days of its appearance. ¹³ Omicron BA.2 has 16 mutations in its RBD alone. Such a high number of mutations is unusual and has been predicted to change the antibody epitopes, and, therefore, to confer significantly higher immune escape properties than the Delta variant. ⁵⁷

Two antibody candidates, namely S2E12,1 a neutralizing antibody bound to the Delta variant,

dominant at the time this investigation was initiated, and H11–D4, which is bound to the WT,⁵⁸ were chosen to examine the immune–escape properties of the VOCs, as well as potential therapies. Additionally, the importance of using fully glycosylated models was investigated to assess whether the complete retinue of glycans is required to reproduce the experimental binding affinity, considering that these polysaccharides have proven crucial in prior studies for recognition and association to the host cell, as well as for escaping the immune response. ^{59,60}

Methods

The following subsections briefly recap the methodology employed in this work and its theoretical underpinnings, and describe the protocols of the simulations reported herein.

Binding free-energy calculations

The formation of a protein–protein complex involves significant conformational changes, encumbering the ergodic sampling of configurations within the simulation time amenable to brute-force MD. Importance sampling algorithms⁶¹ can be used to accelerate the sampling of rare events, such as spontaneous binding. In these algorithms, external forces are applied onto collective variables (CVs), which consist of essential degrees of freedom involved in the reversible association, and can be controlled and monitored in a simulation. For instance, to speed up the reversible binding of two proteins, biasing forces can be applied onto the CV of their separation—i.e., the Euclidean distance between their centers of mass (COMs).

However, considering only the distance between the two COMs does not preclude random tumbling of the two binding partners across the reaction pathway, slowing down the convergence of the separation PMF calculation.⁶¹ To circumvent this shortcoming, appropriate restraints acting on a set of additional CVs, representing the slow degrees of freedom of the complex, are

applied in the course of the separation, as prescribed in the geometrical route introduced by Gumbart et al., 56 the foundation of which can be found in reference 55. These additional CVs are the backbone distance root-mean-square deviations (RMSDs) of the two proteins with respect to the reference, native conformation—i.e., in the complex, the three Euler angles describing their relative orientation, and two additional angles (polar and azimuth) for their relative position. Applying geometrical restraints in the form of soft, harmonic potentials onto these CVs is tantamount to a loss in configurational entropy, corresponding to conformational ($\Delta G_c^{\rm site}$), orientational ($\Delta G_o^{\rm site}$) and positional ($\Delta G_a^{\rm site}$) free-energy contributions, which must be accounted for in the computation of the standard binding free energy, both in the "bulk" (unbound state) and at the "site" (bound state). Therefore, the geometrical route consists of a series of independent PMF calculations determined sequentially with the progressive introduction of restraints as a preamble to performing the separation PMF calculation. The binding free energy can then be expressed as a sum of these different free-energy contributions:

$$\Delta G_{\rm b}^{\circ} = \Delta G_{c}^{\rm bulk} - \Delta G_{c}^{\rm site} - \Delta G_{c}^{\rm site} - \Delta G_{o}^{\rm site} - \Delta G_{a}^{\rm site}(\theta, \phi) + \Delta G_{o}^{\rm bulk} - \frac{1}{\beta} \ln(S^* I^* C^{\circ}) \tag{1}$$

where $\beta=(k_{\rm B}T)^{-1}$, with $k_{\rm B}$, the Boltzmann constant, and T, the temperature. C° denotes the standard concentration of 1 M, that is $C^{\circ}=1/1661$ (Å³). 62 I^{*} is the separation term, and S^{*} is a surface term, which represents the fraction of a sphere of radius r^{*} , centered at the binding site of the reference protein, accessible to its partner, that is,

$$\begin{cases}
I^* = \int_{\text{site}} dr \, e^{-\beta \left(w(r) - w(r^*)\right)} \\
S^* = r^{*2} \int_0^{\pi} d\theta \, \sin\theta \int_0^{2\pi} d\phi \, e^{-\beta u_a}
\end{cases}$$
(2)

Here, r^* is a point far from the binding site, where the proteins no longer interact with each other, u_a is the sum of the harmonic restraint potentials of polar angles θ and ϕ .

In some cases, additional RMSD restraints acting on protein–protein interfacial side chains may be required due to their exposure to the solvent, and the possibility of their isomerization in the course of the separation, resulting in a loss of interaction, and a progressive deterioration of the binding free-energy estimate. ⁵⁶

Computational assays

The structure of the WT:ACE2 complex was taken from the Protein Data Bank (PDB) source 6M0J¹⁰. Our structures of the Alpha, Beta and Delta variants were constructed by introducing single-point mutations in the WT RBD, namely (i) N501Y for the Alpha variant, (ii) N501Y, E484K, K417N for the Beta variant, and (iii) T487K and L452R for the Delta variant^{6,63} using VMD⁶⁴ and called, respectively, Alpha_{model}, Beta_{model} and Delta_{model}.

The Omicron BA.2 variant differs significantly from its fellow VOCs and contains 16 mutations in its RBD alone (G333D, S371F, S373P, S375F, T376A, D405N, R408S, K417N, N440K, S477N, T478K, E484A, Q493R, Q498R, N501Y, and Y505H). A configurational change with a better packing of the N-terminal chain of ACE2 in comparison to the WT has been observed, and could thermodynamically favor intermolecular interactions. Such discrepancy with the WT strain dictated the choice of using the experimental X-ray structure of the BA.2 sub-variant deposited in the PDB (7ZF7).

As glycans were shown to play an important role in recognition and association, ^{59,60} the consequence of their presence on the binding affinity was also investigated in this work. A model of the WT:ACE2 complex with full-length polysaccharide chains was generated using a previously constructed model (see ACE2 Scheme #1 in reference 67) relying on the initial structure 6M17. ⁶⁸ We note that the two complexes in PDBs 6M17 and 6M0J are nearly identical (RMSD of 1.2 Å) and likely represent the same energetic minimum. The antibody assays were prepared with the Charmm-GUI webserver. ⁶⁹ Point mutations in the RBD (viz. T478K, L452R) were introduced to

generate the S2E12:Delta complex by using the WT structure deposited in the PDB (7R6X) as a template. The H11-D4:WT complex was obtained from the PDB (6YZ5).

While the calculations with our models were ongoing, new experimental structures for the Alpha, Beta, and Delta variants were reported. 70-72 As a measure of precaution, we checked our models against these new structures to ensure that the altered interfaces were consistent with all available experimental data. For the Delta variant, the interacting pattern shown by McCallum et al. was identical to ours and the Delta_{model} retained. ⁷⁰ The experimental structure of the Alpha variant was published in the PDB (7EDJ) by Yang et al. 71 A short SMD simulation was performed to correct our interface, and mirror the interaction pattern of their structure in our Alpha_{model} structure. The Beta variant structure was deposited in the PDB 7SY6 in late December 2021 by Mannar et al. 72 An alignment revealed a local rearrangement at the interface centered about residue H34 of ACE2 in the experimental structure, and absent in our model. This conformational change is specific to the Beta variant, and is not present in other VOCs, as documented by the authors. 72 While our initial model of the Beta variant, on the one hand, and the early structure of the WT taken from the Covid-19 Charmm-GUI archive, on the other hand, depart from the more recent experimental structures, we have decided to report the corresponding free-energy calculations to showcase the influence of the starting structure on the binding affinity using both models (WT_{model}, Beta_{model}) and experimental structures (WT_{crvstal}, Beta_{Crvo-EM}).

Molecular dynamics simulations

The macromolecular CHARMM36⁷³ force field and the TIP3P model⁷⁴ were used to describe the proteins and the water, respectively. The zinc ion present in the ACE2 protein was kept due to its catalytic importance in the ACE2 function.⁷⁵ The parameters of the zinc ion were taken from the zinc AMBER force field (ZAFF)⁷⁶ for a cation chelated by two histidine and two glutamate residues, corresponding best to the coordination pattern in our ACE2 structure.

All simulations were performed using the NAMD 3.0 MD engine.⁷⁷ All computational assays corresponded to a physiological concentration of NaCl of 0.15 M. They were minimized for 500 steps, prior to a 100-ns pre-equilibration in the isothermal-isobaric ensemble, keeping the temperature (300 K) and the pressure (1 atm) constant by means of a Langevin thermostat⁷⁸ and the Langevin piston algorithm, 79 respectively. The particle-mesh Ewald (PME) algorithm 80 was utilized to handle long-range electrostatic interactions. Van der Waals and short-range electrostatic interactions were truncated with a smoothed 12-Å spherical cutoff. The equations of motion were integrated with a 2-fs time step. The coordinates and force-field parameters from the preequilibration steps were used as inputs in the binding free-energy estimator 2 (BFEE2), 81 a tool for streamlining and automating the setup of binding free-energy calculations, originally designed to tackle protein-ligand complexes. To expand the BFEE2 applicability to protein-protein complexes, RMSD calculations of the backbone of each protein were included, both in the bulk aqueous medium and at the binding site. The importance-sampling algorithm employed for the computation of the PMFs was the well-tempered extended adaptive biasing force algorithm (WTM-eABF)⁸² as implemented in the collective variable module (Colvars) of NAMD. 83 The PMFs were run sequentially for all complexes, starting from the distance RMSD of the proteins with respect to the native conformation up to the physical separation of two proteins. Only the bound state RMSDs of the Alpha_{model} and both Beta variants required modifications of the default parameters to address convergence issues (see Supporting Information (SI) for additional details). Once all the simulations were completed, BFEE2⁸¹ was invoked again for the post-treatment of the PMFs to extract the individual contributions of the binding affinity, and to infer the final binding free-energy estimate (see SI for details of the computation).

Results and Discussion

Binding free-energy calculations

The binding free-energy estimates for the different complexes are gathered in Table 1, and nearly all match the experimental measurements within chemical accuracy, except for the early WT:ACE2 model. The reason for the significant discrepancy between the theoretical and experimental $\Delta G_{\rm b}^{\circ}$ stems from local differences between the model and the experimental structure. Since models can miss crucial interactions, their use magnifies the vulnerability of free-energy calculations to inadequate initial structures, and the likelihood of erroneous binding-affinity estimates. However, in some cases, such as the Beta variant model in complex with ACE2, the structural differences discussed previously did not affect at first sight the theoretical $\Delta G_{\rm b}^{\circ}$. Replacing key interactions with a number of poorly predicted side-chain interactions could result in a fortuitous cancellation of errors, with no guarantee of recovering the correct network of nonbonded interactions, and, hence, the correct standard binding free energy. It is noteworthy that accurate structure modeling is not only a prerequisite to the geometrical route, but, in general, to all MD-based binding free-energy strategies.

Table 1. Computed binding free energy against experimental values of all studied complexes

| Complexes | $\Delta G_{ m b}^{\circ}$ (kcal/mol) | $\Delta G_{\mathrm{exp}}^{\circ} (\mathrm{kcal/mol})$ |
|-------------------------------|--------------------------------------|--|
| WT _{crystal} :ACE2 | -11.5 ± 0.3 | -11.4^{10} |
| WT _{model} :ACE2 | -6.7 ± 2.3 | -11.4^{10} |
| Alpha _{model} :ACE2 | -12.3 ± 1.2 | -11.6^{84} |
| Beta _{model} :ACE2 | -10.0 ± 1.2 | -11.1^{84} |
| Beta _{Cryo-EM} :ACE2 | -11.0 ± 1.6 | -11.1^{84} |
| Delta _{model} :ACE2 | -9.6 ± 0.5 | -9.9^{70} |
| Omicron BA.2:ACE2 | -11.4 ± 1.3 | -11.5^{66} |
| WT:ACE2 (full-length glycans) | -10.8 ± 0.3 | -11.4^{10} |
| S2E12:Delta | -12.5 ± 0.3 | -12.0^{1} |
| H11-D4:WT | -9.4 ± 0.5 | -9.9^{58} |

Comparing the $\Delta G_{\rm b}^{\circ}$ of all VOCs in complex with ACE2, it is apparent that the Delta variant

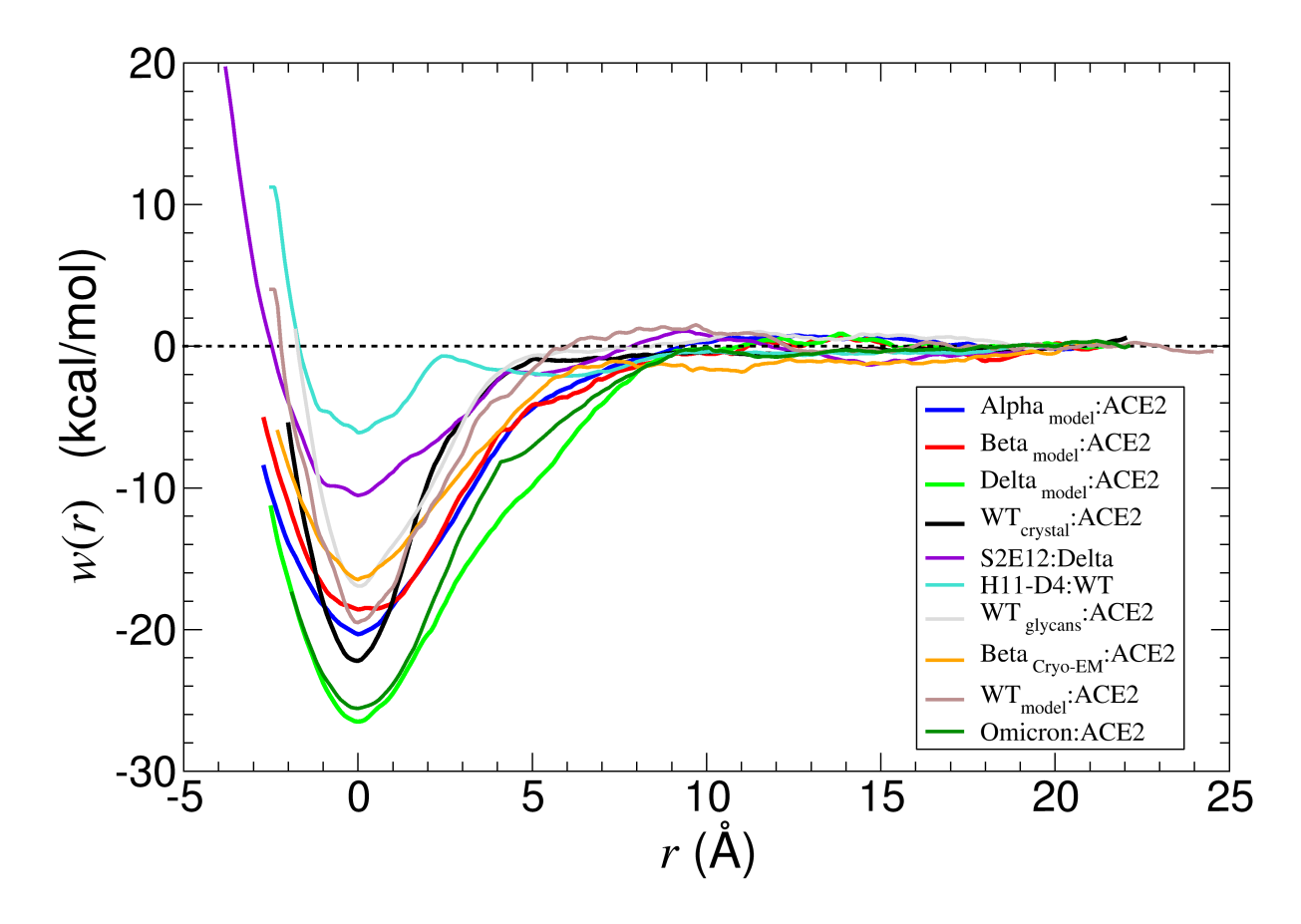


Figure 1. PMFs obtained during the reversible separation of ACE2 and the RBD of the WT (with minimal glycans in black, fully glycosylated in grey and the early model in taupe) and the different variants (Alpha $_{\rm model}$: blue, Beta $_{\rm model}$: red, Beta $_{\rm Cryo-EM}$: orange, Delta $_{\rm model}$: clear green, Omicron BA.2: dark green) or the RBD and antibodies (S2E12:Delta: violet, H11-D4:WT: cyan). All PMFs have been shifted so that the bound state is set to r=0.

possesses the lowest binding affinity for the receptor (viz. -9.6 kcal/mol), which is almost 2 kcal/mol weaker than that of the WT (viz. -11.5 kcal/mol) (see Table 1). Moreover, Mlcochova et al.² showed experimentally that the Delta variant does not exhibit a higher affinity towards human ACE2 than both the Alpha variant (viz. -11.6 kcal/mol)⁸⁴ and the WT. Their findings corroborate our calculations, from whence we can conclude that the Delta variant increases its fitness over other VOCs by relying more on immune escape than on increased affinity. This result explains the rapid prevalence of the Delta variant over previous VOCs, notwithstanding the increased vaccination rate amid the population. 18,85

The Omicron BA.2 variant has been reported both by experimental and theoretical studies to

have either an enhanced affinity, or an affinity similar to that of the Delta variant, causing some debate on the actual affinity of Omicron for ACE2. ^{11,86–90} Our results confirm an affinity close to that of the WT, notwithstanding their very different binding interfaces. As can be seen from Figure 1, the separation PMFs for Delta and Omicron BA.2 are strikingly similar, which could explain the uncertainty on the reported binding affinity of the two VOCs. ^{11,86–90}

As depicted in Figure 1, among all PMFs underlying the separation of the VOCs from ACE2, Delta possesses the largest well depth, in excess of -26 kcal/mol, which is almost 2.5 times the absolute value of the final estimate (viz. -9.6 kcal/mol). This result underscores the importance of accounting for all the degrees of freedom other than the physical separation of the binding partners in standard binding free-energy calculations. More specifically, the PMFs along the RMSDs (see Table S6) contribute significantly to the binding affinity. It is also worth noting that most of the computational effort (viz. 60% of the total simulation time for the WT) was invested in recovering the conformational entropy contributions in the bulk and at the binding site. The Alpha and model Beta (referred to as Beta_{model}) variants correspond to similar PMFs (see Figure 1). Their well depths differ by less than 2 kcal/mol. A possible reason for this discrepancy lies in using the same initial template and the shared N501Y mutation, which significantly increases the binding affinity, as reported in the literature. 19,23,30

Furthermore, when comparing the different free-energy contributions for the variants (see Table S11), we notice that orientational and positional contributions in the bound states are both similar and small when compared to the other contributions. The conformational and the physical separation vary the most between VOCs. The difference in the conformational contribution arises from the mutations that confers differences in the inner flexibility/stability of the proteins. The $WT_{\rm model}$ conformational contribution is significantly higher than that for the rest of the variants due to the need of stronger restraints to assuage convergence issues, as stated in the SI.

The WT:ACE2 complex structure used here is minimally glycosylated, with only one glycan found at four glycosylation sites on ACE2 (i.e., N53, N90, N322, and N546) and one site on the

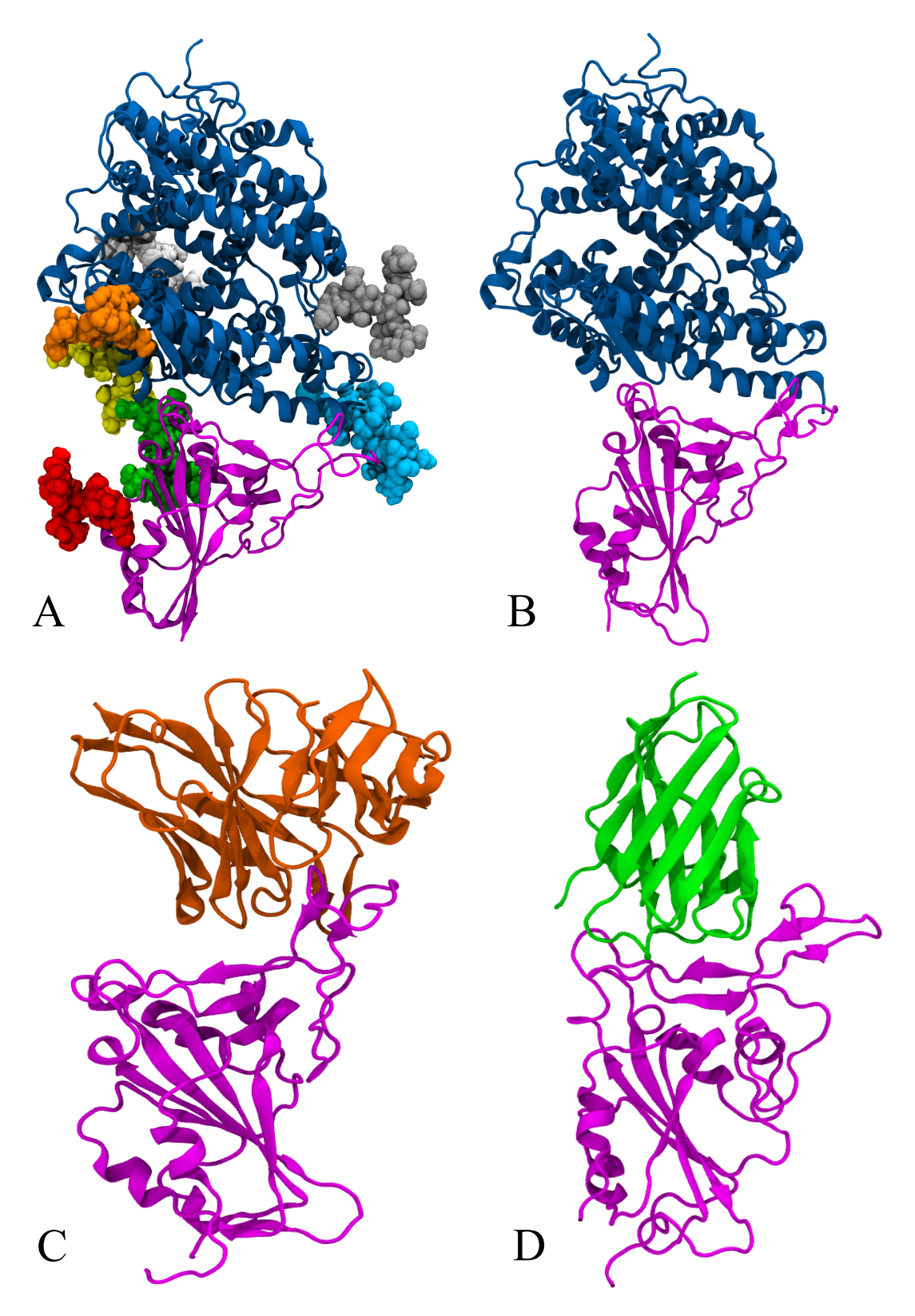


Figure 2. Representation of the binding mode of (A) WT:ACE2 with glycans, (B) WT:ACE2, (C) WT:H11-D4, (D) Delta:S2E12.

RBD (N343). Additional glycans, while present, were not resolved, likely due to their flexibility. To determine the effect of full-length glycans on binding, if any, we repeated the calculation of the binding free energy between the RBD and ACE2 using a fully glycosylated model of the complex constructed previously (see ACE2 Scheme #1 in reference 67). This model has 8–10 sugars at each site—the ones mentioned already, as well as two others on ACE2 (namely, at N103 and N432), as depicted in Figure 2A. Following the same steps as in the other calculations, we found a slightly smaller (about -1 kcal/mol) binding free energy at -10.8 kcal/mol, compared to the minimally glycosylated model (-11.5 kcal/mol). This is in subtle contrast to recent experiments, in which the presence of glycans was found to contribute about +1 kcal/mol to the binding (-10.3 kcal/mol for the fully glycosylated complex, and -9.7 kcal/mol for that devoid of glycans). Regardless, our calculated binding free energy for the fully glycosylated complex falls within the range observed experimentally, which spans $4k_{\rm B}T$ (-9.0 kcal/mol, 92 -10.3 kcal/mol, 91 and -11.4 kcal/mol 10).

To determine the efficiency of antibodies against SARS-CoV-2 variants, we selected two complexes, namely the neutralizing nanobody H11-D4 bound to the WT, ⁵⁸ and the human antibody S2E12 bound to the Delta variant. ¹ The experimental binding free energy taken as the reference in Table 1 for the S2E12:Delta complex was inferred from a neutralization curve reported by MI-cochova et al., ² where the Delta variant exhibits a behavior similar to the WT, thus justifying the use of the WT experimental value for the Delta variant in complex with S2E12. The binding poses of the antibody complexes are depicted in Figure 2. H11-D4 binds the WT by forming several hydrogen bonds (S494:V102, E484:S57, E484:R52, F490:S104, Q493:S104), and a salt bridge (R52:E484). Stacking of Y449 onto N101 also participates in the binding. ⁵⁸ The S2E12 binding site is centered about P486, with a cavity lined with aromatic residues ¹ as shown in Figure 3.

The calculated binding free energies for the antibody complexes matched the experimental data within chemical accuracy (see Table 1). The binding affinity for the H11-D4:WT complex amounts to -9.4 kcal/mol, which is less than that for WT:ACE2 (i.e., -11.5 kcal/mol). These results emphasize the insufficient neutralizing activity of H11-D4 against SARS-CoV-2 in its WT

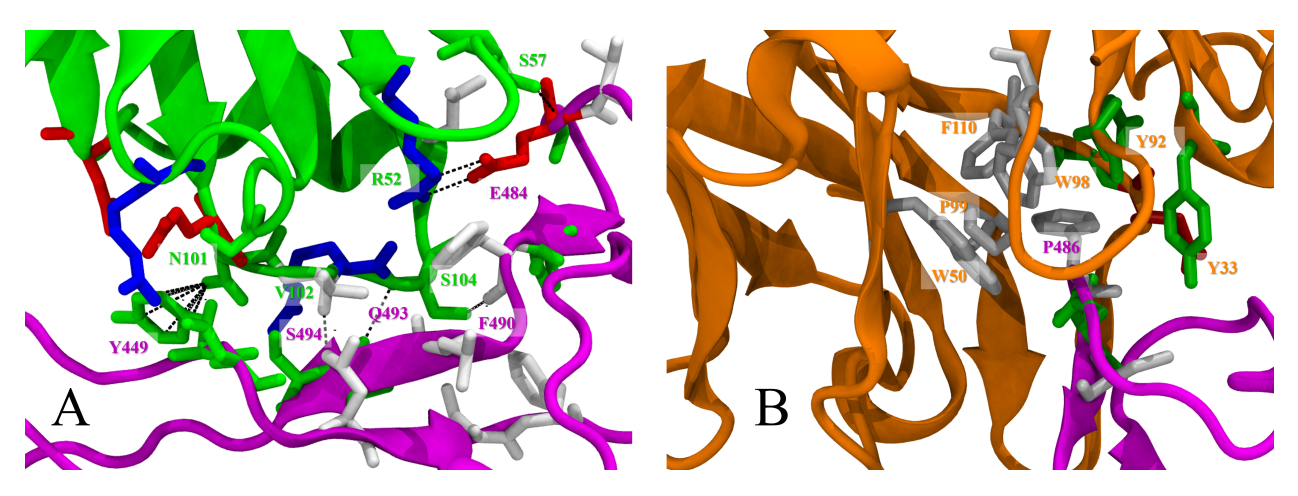


Figure 3. Interaction interfaces of (A) antibody H11-D4 and the WT RBD and (B) antibody S2E12 and the Delta RBD, with salt bridges and hydrogen bonds highlighted with dotted lines.

strain, at least absent for significantly higher concentrations than ACE2. Huo et al.⁵⁸ reached the same conclusion based on the nonconservation of the H11-D4 epitope between SARS-CoV and SARS-CoV-2, from whence they recommended the use of H11-D4 in cocktails of antibodies binding different regions of SARS-CoV-2 to boost the efficiency of the treatment. The binding affinity of S2E12 to the Delta variant reported by Mlcochova et al., 2 was confirmed by our binding free-energy calculations. The large $\Delta G_{\rm h}^{\circ}$ for S2E12:Delta complex, amounting to -12.5 kcal/mol, is appreciably greater than that for Delta: ACE2 (-9.6 kcal/mol). Put together, although the Delta variant does not lean on a strong binding to ACE2, but rather on immunity escape, 2,18 the S2E12 antibody seems to be effective against SARS-CoV-2 infection induced by the Delta variant. Starr et al. showed that unlike other antibodies examined in their study, S2E12 was able to bind to a gamut of SARS-CoV-2 variants. They stated that its efficiency could be linked to the scarcity of S2E12 in polyclonal sera, as well as to the lack of evolutionary pressure by this antibody to SARS-CoV-2. In summary, S2E12 is a therapeutic candidate that could potentially withstand the appearance of new variants, while retaining a reasonable efficacy against the virus. 93 A recent study by Huang et al. demonstrated that among 50 monoclonal antibodies tested, S2E12 was one of only three antibodies that retained sufficient neutralizing properties against Omicron sub-variants (IC50 < 1 μ g/mL), ⁹⁴ confirming our previous statement.

Protein-protein interaction networks

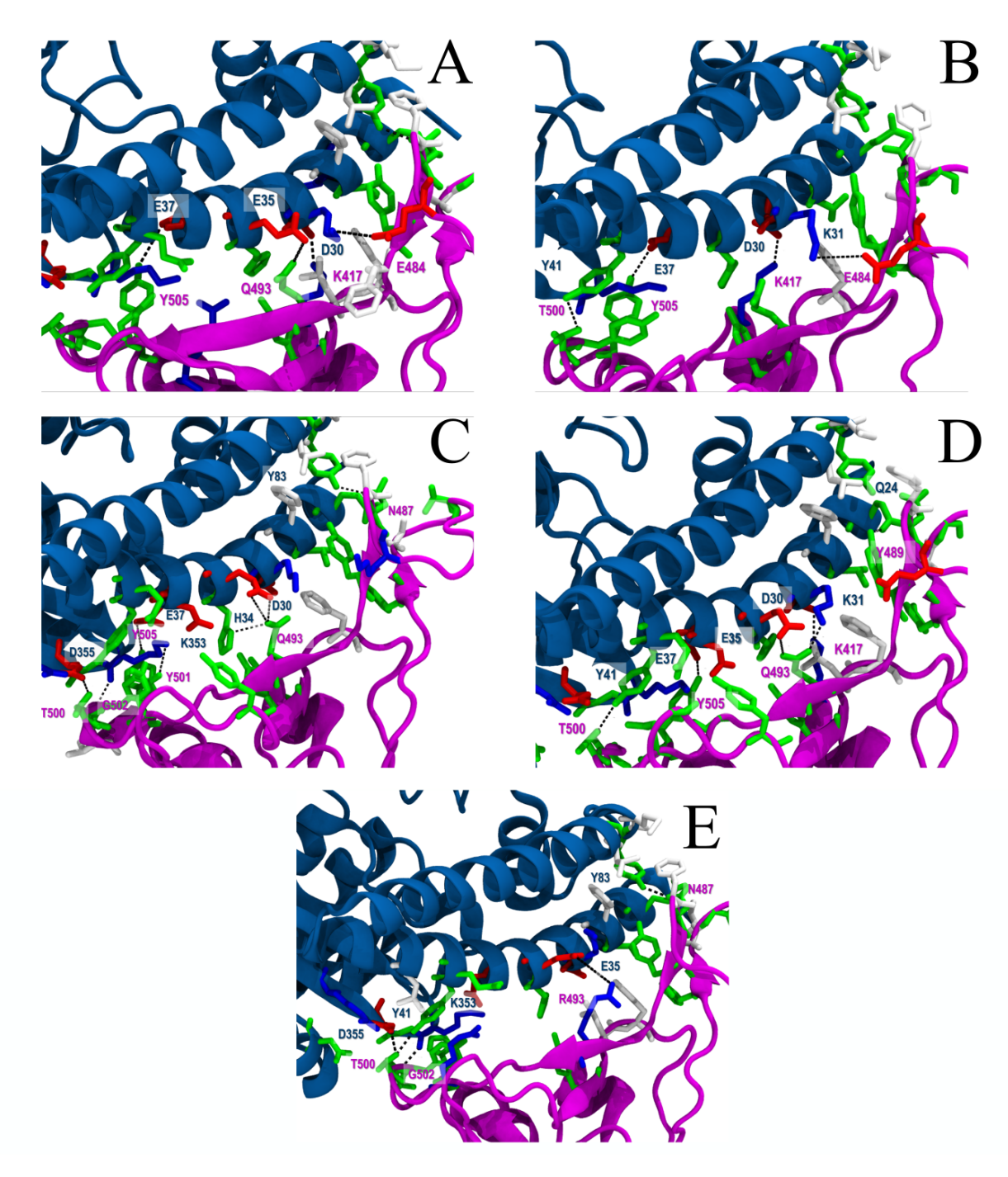


Figure 4. Interaction interface with ACE2 of (A) WT, (B) Alpha, (C) Beta, (D) Delta, and (E) Omicron BA.2 variants with salt bridges and hydrogen bonds highlighted with dotted lines.

To understand the consequences of mutations in terms of binding affinity, we analyzed the separation trajectories in greater detail, focusing on the networks of interactions consisting of salt

bridges and hydrogen bonds. In our simulations, we observed the formation of D30:K417 and K31:E484 salt bridges (see Figures 4 and 5) in Alpha:ACE2, Delta:ACE2 and WT:ACE2 complexes when the two proteins are in intimate contact (i.e., COM distance $< 50 \ \text{Å}$). As shown in Figure 5, the Alpha variant exhibits higher occupancy for both salt bridges. It can partially explain why the Alpha variant has the highest binding affinity towards the human receptor among all VOCs. Interestingly enough, the histograms for the Delta variant and the WT are almost similar insofar as these two salt bridges are concerned. This resemblance could rationalize why the affinity did not increase when the Delta variant emerged. Our theoretical results confirm the observation of Bhattarai et al. 95 on the importance of the presence of these salt bridges in the case of the WT and the Alpha variant. However, these non-covalent interactions are no longer present in the Beta variant owing to the K417N and E484K mutations. According to the experimental data—and to our simulations, the binding free energies of the Alpha and Beta variants are similar.⁸⁴ The loss of the D30:K417 and K31:E484 salt bridges in the Beta variant, either in the Cryo-EM structure (referred to as $Beta_{\mathrm{Cryo-EM}})$ or in the model (Beta_{\mathrm{model}}), might be compensated by the formation of novel interactions, e.g., a salt bridge detected by Socher et al. 96 between K484 and E75. This particular salt bridge was only detected in the case of the $Beta_{Crvo-EM}$:ACE2 complex and in a small number of configurations in our separation trajectory. Luan et al. have also observed the formation of this salt bridge after 190 ns of simulation, and reasoned that exposure to water weakened and even broke this interaction, ²¹ which rationalizes its scarcity in our own simulations. This new interaction could also explain why the loss of K31:E484 and D30:K417 did not result in any significant decrease in the binding affinity for the Beta_{Crvo-EM} variant. This discrepancy in the detection of salt bridges between the two Beta variant structures underscores again the need for an appropriate starting structure.

The most important hydrogen-bond interactions that occurred at the interface between ACE2 and the different VOCs are depicted in Figure 5, where substantial discrepancies in occupancy are visible when the partners are in intimate contact (distance between COMs < 50 Å). For instance, the population of the E24:A475 hydrogen bond is strongly reduced in the different variants (viz.

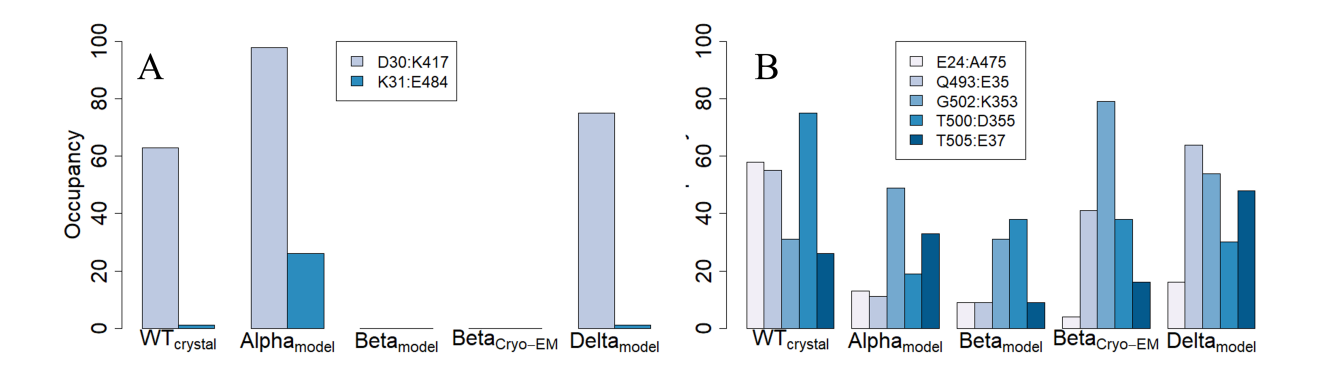


Figure 5. (A) Occupancy of the salt bridges in the separation trajectories for the WT and the studied variants computed at a close center-of-mass distance (<50 Å). (B) Occupancy of the hydrogen bonds in the separation trajectories for the WT and the studied variants computed at a close center-of-mass distance (<50 Å).

58% for the WT against 13%, 9%, 4% and 16% for the Alpha, Beta_{model}, Beta_{Cryo-EM}, and Delta variants, respectively). The Beta variant model exhibits a hydrogen-bond pattern similar to that of its Alpha counterpart for the first three bonds (i.e., E24:A475, Q493:E35, and G502:K353), which is another argument in favor of the similarity of the PMFs, and the use of the same initial template. The discrepant hydrogen-bond occupancy between the two Beta structures is evidenced in Figure 5, which highlights a lower occupancy for all bonds in the case of the model structure, barring the initial one, that is E24:ALA475. This result implies that misplaced side chains in the model may result in a destabilized interface, and explain the ca. 1 kcal/mol difference between their ΔG_b° 's (see Table 1).

The high number of mutations harbored by Omicron in the RBD is responsible for a totally different binding interface, thus preventing a direct comparison of interaction networks between this variant and the other VOCs. A compensation between favorable, e.g., N501Y, and destabilizing mutations, e.g., K417N, is responsible for maintaining appropriate binding to ACE2, while generating significant immune escape, as revealed by structural analysis. ^{66,97} Omicron BA.2 does not possess any of the salt bridges previously mentioned owing to the Q493R, K417N and E484A mutations. However, a new salt bridge formed between E35 and R493 was detected in our simulations. Some hydrogen bonds were conserved when compared to the WT, like G502:K353 and

T500:D355.

Conclusions

The COVID-19 crisis has exerted tremendous pressure on the scientific community to obtain fast and accurate results to help understand and battle the SARS-CoV-2 virus. The syndemic started over two years ago, and a wealth of data has been published during this time interval. Determination of new structures of the VOCs bound to either ACE2 or antibodies has made possible the theoretical investigation reported herein, offering a critical assessment of the predictive power of a state-of-the-art methodology for protein-protein standard binding free-energy calculations. We have applied a rigorous computational protocol leaning on the so-called geometrical route to determine the binding free energies of VOC:ACE2 complexes, where VOCs stand for the RBD of the WT, Alpha, Beta, Delta, and Omicron BA.2 variants, and antibodies: VOC (H11-D4:WT, S2E12:Delta) complexes, and underscored the importance of the contribution arising from all degrees of freedom other than the physical separation of the binding partners, most notably the conformational ones. Except for the model WT:ACE2 complex, the experimental binding free energies of all complexes were reproduced in approximately $1-\mu s$ -long simulations up to chemical accuracy, emphasizing both the robustness and the potency of the method. The Beta variant model failed to yield the experimental affinity, albeit falling within the $k_{\rm B}T$ margin, which stems from fortuitous cancellations of errors rooted in an incorrect starting structure. The discrepancies between the model and the Cryo-EM structures underscore the paramount importance of the starting point. Models—based, for instance, on simple amino-acid replacements, as well as docked structures are often produced in the absence of structural data, but, owing to their questionable accuracy, are of limited use, regardless of how predictive the methodology at hand is, as was demonstrated cogently in this work. Comparing the affinity obtained for all VOCs, using WT:ACE2 as a reference, we established that both the Alpha and the Beta variants rely on an increased affinity for ACE2.

In contrast, the Delta variant has a lower affinity for ACE2, and has spread widely owing to its immune-escape properties. The Omicron variant has a binding affinity similar to that of the WT, albeit harboring a different interaction pattern at the interface, thereby explaining its high degree of immune escape and the rapid prevalence of this variant. The Alpha and the Beta variant share a common mutation, namely N501Y, which explains, at least in part, the resemblance of their PMFs, and, thus, their similar binding affinities. However, the Beta variant has additional specific mutations, viz. E484K and K417N, found to compensate each other, 98 and, as a result, these mutations do not significantly affect its binding free energy when compared to the Alpha variant. 98 Inasmuch as the complexes with an antibody are concerned, the present investigation indicates that S2E12 has a strong affinity for the Delta variant and, thus, represents a potential candidate for COVID-19 therapies, irrespective of the variant at play, being in principle able to withstand the emergence of new mutations. 93 Notwithstanding the vulnerability to the initial structure of MD-based freeenergy calculations, in general, and of the geometrical route, in particular, the latter methodology, when applied rigorously, devoid of shortcuts, constitutes a reliable approach to predict the binding affinity of existing and ever-emerging variants of SARS-CoV-2 towards the host cell, whilst offering valuable atomistic insights into the underlying recognition and association processes.

Acknowledgement

This investigation was supported by the University of Lorraine thought the LUE initiative and by the Agence Nationale de la Recherche (ArtificialIntelligence, ProteaseInAction). Computational resources were also provided through XSEDE (TG-MCB130173), which is supported by the National Science Foundation (NSF; ACI-1548562). This work also used the Hive cluster, which is supported by the NSF (1828187) and is managed by PACE at the Georgia Institute of Technology.

Supporting Information Available

Description of the molecular assemblies, computational details (individual contributions and convergence) of all free-energy calculations.

References

- (1) Starr, T. N.; Czudnochowski, N.; Liu, Z.; Zatta, F.; Park, Y.-J.; Addetia, A.; Pinto, D.; Beltramello, M.; Hernandez, P.; Greaney, A. J. et al. SARS-CoV-2 RBD antibodies that maximize breadth and resistance to escape. *Nature* **2021**, *597*, 97–102.
- (2) Mlcochova, P.; Kemp, S.; Dhar, M. S.; Papa, G.; Meng, B.; Ferreira, I. A. T. M.; Datir, R.; Collier, D. A.; Albecka, A.; Singh, S. et al. SARS-CoV-2 B.1.617.2 Delta variant replication and immune evasion. *Nature* **2021**, *599*, 114–119.
- (3) Wang, C.; Horby, P. W.; Hayden, F. G.; Gao, G. F. A novel coronavirus outbreak of global health concern. *Lancet* **2020**, *395*, 470–473.
- (4) Horton, R. Offline: COVID-19 is not a pandemic. *Lancet* **2020**, *396*, 874.
- (5) WHO Coronavirus (COVID-19) Dashboard. https://covid19.who.int, accessed January 28, 2022.
- (6) Jackson, C. B.; Farzan, M.; Chen, B.; Choe, H. Mechanisms of SARS-CoV-2 entry into cells. *Nat. Rev. Mol. Cell. Biol.* **2022**, *23*, 3–20.
- (7) Yao, H.; Song, Y.; Chen, Y.; Wu, N.; Xu, J.; Sun, C.; Zhang, J.; Weng, T.; Zhang, Z.; Wu, Z. et al. Molecular Architecture of the SARS-CoV-2 Virus. *Cell* **2020**, *183*, 730–738.e13.
- (8) Walls, A. C.; Park, Y.-J.; Tortorici, M. A.; Wall, A.; McGuire, A. T.; Veesler, D. Structure, Function, and Antigenicity of the SARS-CoV-2 Spike Glycoprotein. *Cell* **2020**, *181*, 281–292.e6.
- (9) Shang, J.; Ye, G.; Shi, K.; Wan, Y.; Luo, C.; Aihara, H.; Geng, Q.; Auerbach, A.; Li, F. Structural basis of receptor recognition by SARS-CoV-2. *Nature* **2020**, *581*, 221–224.
- (10) Lan, J.; Ge, J.; Yu, J.; Shan, S.; Zhou, H.; Fan, S.; Zhang, Q.; Shi, X.; Wang, Q.; Zhang, L. et al. Structure of the SARS-CoV-2 spike receptor-binding domain bound to the ACE2 receptor. *Nature* **2020**, *581*, 215–220.

- (11) Hoffmann, M.; Kleine-Weber, H.; Pöhlmann, S. A Multibasic Cleavage Site in the Spike Protein of SARS-CoV-2 Is Essential for Infection of Human Lung Cells. *Mol. Cell* **2020**, 78, 779–784.e5.
- (12) Benton, D. J.; Wrobel, A. G.; Xu, P.; Roustan, C.; Martin, S. R.; Rosenthal, P. B.; Skehel, J. J.; Gamblin, S. J. Receptor binding and priming of the spike protein of SARS-CoV-2 for membrane fusion. *Nature* **2020**, *588*, 327–330.
- (13) Tracking SARS-CoV-2 variants. https://www.who.int/health-topics/typhoid/tracking-SARS-CoV-2-variants, accessed January 28, 2022.
- (14) Liu, C.; Zhou, Q.; Li, Y.; Garner, L. V.; Watkins, S. P.; Carter, L. J.; Smoot, J.; Gregg, A. C.; Daniels, A. D.; Jervey, S. et al. Research and Development on Therapeutic Agents and Vaccines for COVID-19 and Related Human Coronavirus Diseases. ACS Cent. Sci. 2020, 6, 315–331.
- (15) Volkan, E. COVID-19: Structural Considerations for Virus Pathogenesis, Therapeutic Strategies and Vaccine Design in the Novel SARS-CoV-2 Variants Era. *Mol. Biotechnol.* **2021**, *63*, 885–897.
- (16) CDC, Coronavirus Disease 2019 (COVID-19). 2020; https://www.cdc.gov/coronavirus/2019-ncov/variants/variant-classifications.html, accessed February 21, 2022.
- (17) Gobeil, S. M.-C.; Janowska, K.; McDowell, S.; Mansouri, K.; Parks, R.; Stalls, V.; Kopp, M. F.; Manne, K.; Li, D.; Wiehe, K. et al. Effect of natural mutations of SARS-CoV-2 on spike structure, conformation, and antigenicity. *Science* **2021**, *373*, eabi6226.
- (18) Zhang, J.; Xiao, T.; Cai, Y.; Lavine, C. L.; Peng, H.; Zhu, H.; Anand, K.; Tong, P.; Gautam, A.; Mayer, M. L. et al. Membrane fusion and immune evasion by the spike protein of SARS-CoV-2 Delta variant. *Science* **2021**, *374*, 1353–1360.

- (19) Alaofi, A. L.; Shahid, M. Mutations of SARS-CoV-2 RBD May Alter Its Molecular Structure to Improve Its Infection Efficiency. *Biomolecules* **2021**, *11*, 1273.
- (20) Harvey, W. T.; Carabelli, A. M.; Jackson, B.; Gupta, R. K.; Thomson, E. C.; Harrison, E. M.; Ludden, C.; Reeve, R.; Rambaut, A.; COVID-19 Genomics UK (COG-UK) Consortium, et al. SARS-CoV-2 variants, spike mutations and immune escape. *Nat. Rev. Microbiol.* 2021, 19, 409–424.
- (21) Luan, B.; Huynh, T. Insights into SARS-CoV-2's Mutations for Evading Human Antibodies: Sacrifice and Survival. *J. Med. Chem.* **2022**, *65*, 2820–2826.
- (22) Chen, C.; Boorla, V. S.; Banerjee, D.; Chowdhury, R.; Cavener, V. S.; Nissly, R. H.; Gontu, A.; Boyle, N. R.; Vandegrift, K.; Nair, M. S. et al. Computational prediction of the effect of amino acid changes on the binding affinity between SARS-CoV-2 spike RBD and human ACE2. *Proc. Natl. Acad. Sci. U. S. A.* **2021**, *118*, e2106480118.
- (23) Fratev, F. N501Y and K417N Mutations in the Spike Protein of SARS-CoV-2 Alter the Interactions with Both hACE2 and Human-Derived Antibody: A Free Energy of Perturbation Retrospective Study. *J. Chem. Inf. Model.* **2021**, *61*, 6079–6084.
- (24) Villoutreix, B. O.; Calvez, V.; Marcelin, A.-G.; Khatib, A.-M. In Silico Investigation of the New UK (B.1.1.7) and South African (501Y.V2) SARS-CoV-2 Variants with a Focus at the ACE2–Spike RBD Interface. *Int. J. Mol. Sci.* **2021**, 22, 1695.
- (25) Chodera, J. D.; Mobley, D. L.; Shirts, M. R.; Dixon, R. W.; Branson, K.; Pande, V. S. Alchemical free energy methods for drug discovery: progress and challenges. *Curr. Opin. Struct. Biol.* **2011**, *21*, 150–160.
- (26) Pohorille, A.; Jarzynski, C.; Chipot, C. Good Practices in Free-Energy Calculations. *J. Phys. Chem. B* **2010**, *114*, 10235–10253.

- (27) Jorgensen, W. L.; Thomas, L. L. Perspective on Free-Energy Perturbation Calculations for Chemical Equilibria. *J. Chem. Theory. Comput.* **2008**, *4*, 869–876.
- (28) Jorgensen, W. L.; Ravimohan, C. Monte Carlo simulation of differences in free energies of hydration. *J. Chem. Phys.* **1985**, *83*, 3050–3054.
- (29) Zwanzig, R. W. High-Temperature Equation of State by a Perturbation Method. I. Nonpolar Gases. *J. Chem. Phys.* **1954**, 22, 1420–1426.
- (30) Pavlova, A.; Zhang, Z.; Acharya, A.; Lynch, D. L.; Pang, Y. T.; Mou, Z.; Parks, J. M.; Chipot, C.; Gumbart, J. C. Machine Learning Reveals the Critical Interactions for SARS-CoV-2 Spike Protein Binding to ACE2. J. Phys. Chem. Lett. 2021, 12, 5494–5502.
- (31) Smaoui, M. R.; Yahyaoui, H. Unraveling the stability landscape of mutations in the SARS-CoV-2 receptor-binding domain. *Sci Rep* **2021**, *11*, 9166.
- (32) Zou, J.; Yin, J.; Fang, L.; Yang, M.; Wang, T.; Wu, W.; Bellucci, M. A.; Zhang, P. Computational Prediction of Mutational Effects on SARS-CoV-2 Binding by Relative Free Energy Calculations. *J. Chem. Inf. Model.* **2020**, *60*, 5794–5802.
- (33) Izrailev, S.; Stepaniants, S.; Isralewitz, B.; Kosztin, D.; Lu, H.; Molnar, F.; Wriggers, W.; Schulten, K. Steered Molecular Dynamics. Computational Molecular Dynamics: Challenges, Methods, Ideas. Berlin, Heidelberg, 1999; pp 39–65.
- (34) Kim, S.; Liu, Y.; Lei, Z.; Dicker, J.; Cao, Y.; Zhang, X. F.; Im, W. Differential Interactions between Human ACE2 and Spike RBD of SARS-CoV-2 Variants of Concern. *J. Chem. Theory Comput.* **2021**, *17*, 7972–7979.
- (35) Koehler, M.; Ray, A.; Moreira, R. A.; Juniku, B.; Poma, A. B.; Alsteens, D. Molecular insights into receptor binding energetics and neutralization of SARS-CoV-2 variants. *Nat. Commun.* **2021**, *12*, 6977.

- (36) Fotiadis, D.; Scheuring, S.; Müller, S. A.; Engel, A.; Müller, D. J. Imaging and manipulation of biological structures with the AFM. *Micron* **2002**, *33*, 385–397.
- (37) Jarzynski, C. Nonequilibrium Equality for Free Energy Differences. *Phys. Rev. Lett.* **1997**, 78, 2690–2693.
- (38) Park, S.; Khalili-Araghi, F.; Tajkhorshid, E.; Schulten, K. Free energy calculation from steered molecular dynamics simulations using Jarzynski's equality. *J. Chem. Phys.* **2003**, *119*, 3559–3566.
- (39) Garcia-Iriepa, C.; Hognon, C.; Francés-Monerris, A.; Iriepa, I.; Miclot, T.; Barone, G.; Monari, A.; Marazzi, M. Thermodynamics of the interaction between the spike protein of severe acute respiratory syndrome- coronavirus-2 and the receptor of human angiotensin converting enzyme 2. Effects of possible ligands. *J. Phys. Chem. Lett.* 2020, 11, 9272–9281.
- (40) Fu, H.; Zhang, H.; Chen, H.; Shao, X.; Chipot, C.; Cai, W. Zooming across the Free-Energy Landscape: Shaving Barriers, and Flooding Valleys. *J. Phys. Chem. Lett.* **2018**, *9*, 4738–4745.
- (41) Ngo, V. A.; Jha, R. K. Identifying key determinants and dynamics of SARS-CoV-2/ACE2 tight interaction. *PLoS One* **2021**, *16*, e0257905.
- (42) Chakraborty, S. E484K and N501Y SARS-CoV 2 spike mutants Increase ACE2 recognition but reduce affinity for neutralizing antibody. *Int. Immunopharmacol.* **2022**, *102*, 108424.
- (43) Torrie, G. M.; Valleau, J. P. Monte Carlo study of phase separating liquid mixture by umbrella sampling. *J. Chem. Phys.* **1977**, *66*, 1402–1408.
- (44) Kumar, S.; Bouzida, D.; Swendsen, R. H.; Kollman, P. A.; Rosenberg, J. M. The weighted histogram analysis method for free energy calculations on biomolecules. I. The method. *J. Comput. Chem.* **1992**, *13*, 1011–1021.
- (45) Souaille, M.; Roux, B. Extension to the weighted histogram analysis method: combining umbrella sampling with free energy calculations. *Comput. Phys. Commun.* **2001**, *135*, 40–57.

- (46) Onufriev, A. V.; Case, D. A. Generalized Born Implicit Solvent Models for Biomolecules. *Annu. Rev. Biophys.* **2019**, *48*, 275–296.
- (47) Srinivasan, J.; Cheatham, T. E.; Cieplak, P.; Kollman, P. A.; Case, D. A. Continuum Solvent Studies of the Stability of DNA, RNA, and Phosphoramidate-DNA Helices. *J. Am. Chem. Soc.* **1998**, *120*, 9401–9409.
- (48) Im, W.; Beglov, D.; Roux, B. Continuum solvation model: Computation of electrostatic forces from numerical solutions to the Poisson-Boltzmann equation. *Comput. Phys. Commun.* **1998**, *111*, 59–75.
- (49) Lee, M. S.; Olson, M. A. Calculation of Absolute Protein-Ligand Binding Affinity Using Path and Endpoint Approaches. *Biophys. J.* **2006**, *90*, 864–877.
- (50) Homeyer, N.; Gohlke, H. Free Energy Calculations by the Molecular Mechanics Poisson-Boltzmann Surface Area Method. *Mol. Inform.* **2012**, *31*, 114–122.
- (51) Istifli, E. S.; Netz, P. A.; Sihoglu Tepe, A.; Sarikurkcu, C.; Tepe, B. Understanding the molecular interaction of SARS-CoV-2 spike mutants with ACE2 (angiotensin converting enzyme 2). *J. Biomol. Struct. Dyn.* 2021, 0, 1–12.
- (52) Zhou, W.; Xu, C.; Wang, P.; Luo, M.; Xu, Z.; Cheng, R.; Jin, X.; Guo, Y.; Xue, G.; Juan, L. et al. N439K Variant in Spike Protein Alter the Infection Efficiency and Antigenicity of SARS-CoV-2 Based on Molecular Dynamics Simulation. *Front. Cell Dev. Biol.* 2021, 9, 697035.
- (53) Verma, J.; Subbarao, N. Insilico study on the effect of SARS-CoV-2 RBD hotspot mutants' interaction with ACE2 to understand the binding affinity and stability. *Virology* **2021**, *561*, 107–116.
- (54) Khan, A.; Wei, D.-Q.; Kousar, K.; Abubaker, J.; Ahmad, S.; Ali, J.; Al-Mulla, F.; Ali, S. S.; Nizam-Uddin, N.; Sayaf, A. M. et al. Preliminary Structural Data Revealed That the SARS-

- CoV-2 B.1.617 Variant's RBD Binds to ACE2 Receptor Stronger Than the Wild Type to Enhance the Infectivity. *ChemBioChem* **2021**, 22, 2641–2649.
- (55) Woo, H.-J.; Roux, B. Calculation of absolute protein–ligand binding free energy from computer simulations. *Proc. Natl. Acad. Sci. U. S. A.* **2005**, *102*, 6825–6830.
- (56) Gumbart, J. C.; Roux, B.; Chipot, C. Efficient determination of protein-protein standard binding free energies from first principles. *J. Chem. Theory Comput.* **2013**, *9*, 3789–3798.
- (57) Xiong, D.; Zhao, X.; Luo, S.; Cong, Y.; Zhang, J. Z. H.; Duan, L. Immune Escape Mechanisms of SARS-CoV-2 Delta and Omicron Variants against Two Monoclonal Antibodies That Received Emergency Use Authorization. J. Phys. Chem. Lett. 2022, 13, 6064–6073.
- (58) Huo, J.; Le Bas, A.; Ruza, R. R.; Duyvesteyn, H. M. E.; Mikolajek, H.; Malinauskas, T.; Tan, T. K.; Rijal, P.; Dumoux, M.; Ward, P. N. et al. Neutralizing nanobodies bind SARS-CoV-2 spike RBD and block interaction with ACE2. *Nat. Struct. Mol. Biol.* 2020, 27, 846–854.
- (59) Casalino, L.; Gaieb, Z.; Goldsmith, J. A.; Hjorth, C. K.; Dommer, A. C.; Harbison, A. M.; Fogarty, C. A.; Barros, E. P.; Taylor, B. C.; McLellan, J. S. et al. Beyond Shielding: The Roles of Glycans in the SARS-CoV-2 Spike Protein. ACS Cent. Sci. 2020, 6, 1722–1734.
- (60) Sztain, T.; Ahn, S.-H.; Bogetti, A. T.; Casalino, L.; Goldsmith, J. A.; Seitz, E.; McCool, R. S.; Kearns, F. L.; Acosta-Reyes, F.; Maji, S. et al. A glycan gate controls opening of the SARS-CoV-2 spike protein. *Nat. Chem.* 2021, *13*, 963–968.
- (61) Chipot, C., Pohorille, A., Eds. *Free energy calculations. Theory and applications in chemistry and biology*; Springer Verlag, 2007.
- (62) Deng, Y.; Roux, B. Calculation of Standard Binding Free Energies: Aromatic Molecules in the T4 Lysozyme L99A Mutant. *J. Chem. Theory Comput.* **2006**, 2, 1255–1273.

- (63) Chakraborty, C.; Bhattacharya, M.; Sharma, A. R. Present variants of concern and variants of interest of severe acute respiratory syndrome coronavirus 2: Their significant mutations in S-glycoprotein, infectivity, re-infectivity, immune escape and vaccines activity. Rev. Med. Virol. 2022, 32, e2270.
- (64) Humphrey, W.; Dalke, A.; Schulten, K. VMD Visual Molecular Dynamics. *J. Mol. Graph.* **1996**, *14*, 33–38.
- (65) Zhao, X.; Xiong, D.; Luo, S.; Duan, L. Origin of the tight binding mode to ACE2 triggered by multi-point mutations in the omicron variant: a dynamic insight. *Phys. Chem. Chem. Phys.* 2022, 24, 8724–8737.
- (66) Nutalai, R.; Zhou, D.; Tuekprakhon, A.; Ginn, H. M.; Supasa, P.; Liu, C.; Huo, J.; Mentzer, A. J.; Duyvesteyn, H. M. E.; Dijokaite-Guraliuc, A. et al. Potent cross-reactive antibodies following Omicron breakthrough in vaccinees. *Cell* 2022, 185, 2116–2131.e18.
- (67) Acharya, A.; Lynch, D. L.; Pavlova, A.; Pang, Y. T.; Gumbart, J. C. ACE2 glycans preferentially interact with SARS-CoV-2 over SARS-CoV. *Chem. Commun.* **2021**, *57*, 5949–5952.
- (68) Yan, R.; Zhang, Y.; Li, Y.; Xia, L.; Guo, Y.; Zhou, Q. Structural basis for the recognition of SARS-CoV-2 by full-length human ACE2. *Science* **2020**, *367*, 1444–1448.
- (69) Jo, S.; Kim, T.; Iyer, V. G.; Im, W. CHARMM-GUI: A web-based graphical user interface for CHARMM. *J. Comput. Chem.* **2008**, *29*, 1859–1865.
- (70) McCallum, M.; Walls, A. C.; Sprouse, K. R.; Bowen, J. E.; Rosen, L. E.; Dang, H. V.; Marco, A. D.; Franko, N.; Tilles, S. W.; Logue, J. et al. Molecular basis of immune evasion by the Delta and Kappa SARS-CoV-2 variants. *Science* 2021, 374, 1621–1626.
- (71) Yang, T.-J.; Yu, P.-Y.; Chang, Y.-C.; Liang, K.-H.; Tso, H.-C.; Ho, M.-R.; Chen, W.-Y.; Lin, H.-T.; Wu, H.-C.; Hsu, S.-T. D. Effect of SARS-CoV-2 B.1.1.7 mutations on spike protein structure and function. *Nat. Struct. Mol. Biol.* **2021**, *28*, 731–739.

- (72) Mannar, D.; Saville, J. W.; Zhu, X.; Srivastava, S. S.; Berezuk, A. M.; Zhou, S.; Tuttle, K. S.; Kim, A.; Li, W.; Dimitrov, D. S. et al. Structural analysis of receptor binding domain mutations in SARS-CoV-2 variants of concern that modulate ACE2 and antibody binding. *Cell Rep.* 2021, 37, 110156.
- (73) Huang, J.; MacKerell, A. D. CHARMM36 all-atom additive protein force field: Validation based on comparison to NMR data. *J. Comput. Chem.* **2013**, *34*, 2135–2145.
- (74) Mark, P.; Nilsson, L. Structure and Dynamics of the TIP3P, SPC, and SPC/E Water Models at 298 K. *J. Phys. Chem. A* **2001**, *105*, 9954–9960.
- (75) Polak, Y.; Speth, R. C. Metabolism of angiotensin peptides by angiotensin converting enzyme 2 (ACE2) and analysis of the effect of excess zinc on ACE2 enzymatic activity. *Peptides* **2021**, *137*, 170477.
- (76) Peters, M. B.; Yang, Y.; Wang, B.; Füsti-Molnár, L.; Weaver, M. N.; Merz, K. M. Structural Survey of Zinc-Containing Proteins and Development of the Zinc AMBER Force Field (ZAFF). J. Chem. Theory Comput. 2010, 6, 2935–2947.
- (77) Phillips, J. C.; Hardy, D. J.; Maia, J. D. C.; Stone, J. E.; Ribeiro, J. V.; Bernardi, R. C.; Buch, R.; Fiorin, G.; Hénin, J.; Jiang, W. et al. Scalable molecular dynamics on CPU and GPU architectures with NAMD. *J. Chem. Phys.* **2020**, *153*, 044130.
- (78) Uhlenbeck, G. E.; Ornstein, L. S. On the Theory of the Brownian Motion. *Phys. Rev.* **1930**, 36, 823–841.
- (79) Feller, S. E.; Zhang, Y.; Pastor, R. W.; Brooks, B. R. Constant pressure molecular dynamics simulation: The Langevin piston method. *J. Chem. Phys.* **1995**, *103*, 4613–4621.
- (80) Darden, T.; York, D.; Pedersen, L. Particle mesh Ewald: An $N \cdot \log(N)$ method for Ewald sums in large systems. *J. Chem. Phys.* **1993**, 98, 10089–10092.

- (81) Fu, H.; Chen, H.; Cai, W.; Shao, X.; Chipot, C. BFEE2: Automated, Streamlined, and Accurate Absolute Binding Free-Energy Calculations. *J. Chem. Inf. Model.* **2021**, *61*, 2116–2123.
- (82) Fu, H.; Shao, X.; Cai, W.; Chipot, C. Taming rugged free-energy landscapes using an average force. *Acc. Chem. Res.* **2019**, *52*, 3254–3264.
- (83) Fiorin, G.; Klein, M. L.; Hénin, J. Using collective variables to drive molecular dynamics simulations. *Mol. Phys.* **2013**, *111*, 3345–3362.
- (84) Han, P.; Su, C.; Zhang, Y.; Bai, C.; Zheng, A.; Qiao, C.; Wang, Q.; Niu, S.; Chen, Q.; Zhang, Y. et al. Molecular insights into receptor binding of recent emerging SARS-CoV-2 variants. *Nat. Commun.* **2021**, *12*, 6103.
- (85) Edara, V.-V.; Pinsky, B. A.; Suthar, M. S.; Lai, L.; Davis-Gardner, M. E.; Floyd, K.; Flowers, M. W.; Wrammert, J.; Hussaini, L.; Ciric, C. R. et al. Infection and Vaccine-Induced Neutralizing-Antibody Responses to the SARS-CoV-2 B.1.617 Variants. *N. Engl. J. Med.* **2021**, *385*, 664–666.
- (86) Wu, L.; Zhou, L.; Mo, M.; Liu, T.; Wu, C.; Gong, C.; Lu, K.; Gong, L.; Zhu, W.; Xu, Z. SARS-CoV-2 Omicron RBD shows weaker binding affinity than the currently dominant Delta variant to human ACE2. *Sig. Transduct. Target. Ther.* **2022**, *7*, 8.
- (87) Zhang, X.; Wu, S.; Wu, B.; Yang, Q.; Chen, A.; Li, Y.; Zhang, Y.; Pan, T.; Zhang, H.; He, X. SARS-CoV-2 Omicron strain exhibits potent capabilities for immune evasion and viral entrance. *Sig. Transduct. Target. Ther.* **2021**, *6*, 430.
- (88) Kim, S.; Liu, Y.; Ziarnik, M.; Cao, Y.; Zhang, X. F.; Im, W. Binding of Human ACE2 and RBD of Omicron Enhanced by Unique Interaction Patterns Among SARS-CoV-2 Variants of Concern. *bioRxiv* **2022**, 2022.01.24.477633.
- (89) Nguyen, H. L.; Thai, N. Q.; Nguyen, P. H.; Li, M. S. SARS-CoV-2 Omicron Variant Binds

- to Human Cells More Strongly than the Wild Type: Evidence from Molecular Dynamics Simulation. *J. Phys. Chem. B* **2022**, *126*, 4669–4678.
- (90) Hong, Q.; Han, W.; Li, J.; Xu, S.; Wang, Y.; Xu, C.; Li, Z.; Wang, Y.; Zhang, C.; Huang, Z. et al. Molecular basis of receptor binding and antibody neutralization of Omicron. *Nature* **2022**, *604*, 546–552.
- (91) Huang, Y.; Harris, B. S.; Minami, S. A.; Jung, S.; Shah, P. S.; Nandi, S.; McDonald, K. A.; Faller, R. SARS-CoV-2 spike binding to ACE2 is stronger and longer ranged due to glycan interaction. *Biophys. J.* **2022**, *121*, 79–90.
- (92) Wrapp, D.; Wang, N.; Corbett, K. S.; Goldsmith, J. A.; Hsieh, C. L.; Abiona, O.; Graham, B. S.; McLellan, J. S. Cryo-EM structure of the 2019-nCoV spike in the prefusion conformation. *Science* **2020**, *367*, 1260–1263.
- (93) Tortorici, M. A.; Beltramello, M.; Lempp, F. A.; Pinto, D.; Dang, H. V.; Rosen, L. E.; Mc-Callum, M.; Bowen, J.; Minola, A.; Jaconi, S. et al. Ultrapotent human antibodies protect against SARS-CoV-2 challenge via multiple mechanisms. *Science* **2020**, *370*, 950–957.
- (94) Huang, M.; Wu, L.; Zheng, A.; Xie, Y.; He, Q.; Rong, X.; Han, P.; Du, P.; Han, P.; Zhang, Z. et al. Atlas of currently available human neutralizing antibodies against SARS-CoV-2 and escape by Omicron sub-variants BA.1/BA.1.1/BA.2/BA.3. *Immunity* **2022**,
- (95) Bhattarai, N.; Baral, P.; Gerstman, B. S.; Chapagain, P. P. Structural and Dynamical Differences in the Spike Protein RBD in the SARS-CoV-2 Variants B.1.1.7 and B.1.351. *J. Phys. Chem. B* **2021**, *125*, 7101–7107.
- (96) Socher, E.; Conrad, M.; Heger, L.; Paulsen, F.; Sticht, H.; Zunke, F.; Arnold, P. Computational decomposition reveals reshaping of the SARS-CoV-2–ACE2 interface among viral variants expressing the N501Y mutation. *J. Cell. Biochem.* **2021**, *122*, 1863–1872.

- (97) Mannar, D.; Saville, J. W.; Zhu, X.; Srivastava, S. S.; Berezuk, A. M.; Tuttle, K. S.; Marquez, A. C.; Sekirov, I.; Subramaniam, S. SARS-CoV-2 Omicron variant: Antibody evasion and cryo-EM structure of spike protein–ACE2 complex. *Science* **2022**, *375*, 760–764.
- (98) Barton, M. I.; MacGowan, S. A.; Kutuzov, M. A.; Dushek, O.; Barton, G. J.; van der Merwe, P. A. Effects of common mutations in the SARS-CoV-2 Spike RBD and its ligand, the human ACE2 receptor on binding affinity and kinetics. *eLife* **2021**, *10*, e70658.